First-principles simulations of 2-D semiconductor devices: mobility, *I-V* characteristics, and contact resistance

M. Luisier*, A. Szabo*, C. Stieger*, C. Klinkert*, S. Brück*, A. Jain†, and L. Novotny†
*Integrated Systems Laboratory (ETH Zurich) / †Photonics Laboratory (ETH Zurich)
Email: mluisier@iis.ee.ethz.ch, Phone: +41 44 632 5333, Fax: +41 44 632 1194, 8092 Zurich, Switzerland

***Abstract*— We report in this paper *ab-initio* quantum transport simulations of different types of single-layer 2-D semiconductors: transition metal and group IV dichalcogenides in the 2H or 1T phase as well as black phosphorus. The electron and hole phonon-limited mobilities of eight selected 2-D crystals are first analyzed before using these materials as n- or p-type channels of ultra-scaled single-gate transistors, computing their *I-V* characteristics in the presence of electron-phonon scattering, and comparing them to each other. Finally, the properties of metal-MoS_2 contacts are investigated. It is revealed that the current tends to flow at the edge of the metal layer before entering the semiconductor, thus limiting the injection efficiency.**

I. Introduction

Following the initial discovery of graphene in 2004 [1] several other 2-D materials have since received wide attention from the scientific community. This is the case, for example, of transition metal dichalcogenides (TMDs), e.g. MoX_2 [2] and WX_2 [3], where X is a chalcogen, of group IV dichalcogenides such as SnX_2 [4], or of black phosphorus (BP) [5]. Different crystal structures exist for these 2-D materials such as trigonal prismatic (2H) or octahedral (1T) for dichalcogenide components and orthorhombic for BP. Several 2-D monolayers exhibit suitable mobility values for logic applications (>100 cm^2/Vs at room temperature) [6], while the ON/OFF current ratio of transistors with a 2-D channel can reach 10^6 or more [2].

Although already impressive these results could be further improved if the quality of the underlying 2-D crystals would increase through a reduction of the defect concentration and of charged impurity scattering [7]. Also, the source and drain contact resistances of transistors implementing a 2-D single-layer semiconductor channel should be significantly decreased. They currently lie in the range of several $k\Omega \cdot \mu$m's and severely limit the operation of such devices [8].

The goal of this paper is to shed light on the intrinsic, phonon-limited, mobility and *I-V* characteristics of various 2-D materials in a monolayer configuration (MoS_2, $MoSe_2$, $MoTe_2$, WS_2, WSe_2, SnS_2, and black phosphorus with two different transport directions), to identify the most promising candidates, to determine the mechanisms responsible for the large contact resistances, and to compare the performance of three different contact metals to each other (Titanium, Scandium, and Gold). For that purpose an *ab-initio* (from first-principles) simulation approach will be used. It is briefly summarized in Section II. Device results are presented in Section III, whereas conclusions are drawn in Section IV.

II. Approach

All simulations reported in this paper have been performed with an atomistic quantum transport solver capable of going beyond the ballistic limit and including electron-phonon interactions [9]. Due to the impracticality of the effective mass approximation and the difficulty of creating empirical tight-binding parameters to reproduce the bandstructure of most TMDs, an alternative scheme has been developed and is applied here. It only requires the atomic coordinates of a representative unit cell from which the entire device structure can be reconstructed through translations.

The idea consists in calculating the electronic structure of the chosen unit cell with a density-functional theory (DFT) package such as VASP [10], converting the plane-wave output into a set of maximally localized Wannier functions (MLWFs) through a unitary transformation [11], producing a tight-binding-like Hamiltonian matrix based on MLWFs, and finally loading it into a dissipative quantum transport code to simulate 2-D devices [12]. In this fully *ab-initio* approach the exchange-correlation functional has been modeled within the general gradient approximation (GGA) and the PBE parameterization [13], except for black phosphorus where HSE06 hybrid functionals have been used [14]. The phonon frequencies and eigenmodes have been obtained through density-functional perturbation theory (DFPT) [15]. As compared to Refs. [16] and [17], the computation of the scattering self-energies has been extended to include beyond nearest-neighbor interactions, as the MLWF Hamiltonian.

III. Results

The investigated device and crystal structures are displayed in Fig. 1. A single-gate transistor with a gate length L_g=10.7 nm and a supply voltage V_{DD}=0.67 V has been designed according to the ITRS specifications for next-generation technology nodes where 2-D materials might play a key role [16]. The eight monolayer semiconductors mentioned above build the channel of this ultra-scaled logic switch. Their electron and hole effective masses at the band edges have been extracted from DFT bandstructures and are given in Fig. 2(a).

By computing the channel resistance of samples with different lengths and by applying the "dR/dL" method [18] the low-field mobility of the considered 2-D materials can be evaluated as a function of the carrier concentration. Only electron-phonon interactions are taken into account, not charge impurity scattering. Hence, what is shown in Fig. 2(b-c) is the phonon-limited hole and electron mobility. It can be seen

978-1-5090-3902-9/16/$31.00 ©2016 IEEE

that (i) the W-based components have larger mobilities than the Mo-based ones because of their smaller effective masses and larger ion masses, which reduces their phonon oscillation amplitudes and scattering rates, (ii) black phosphorus with transport along the Γ-X axis offers the highest hole mobility, and (iii) the electron mobility of MoS_2 is close to other theoretical calculations relying on a different method [19].

The intrinsic I_d-V_{gs} transfer characteristics of the various 2-D transistors are plotted in Fig. 3, together with the resulting ON-currents. Electron-phonon scattering is included to avoid negative differential resistances [12]. With an inverse subthreshold slope SS=80±4 mV/dec all devices maintain a good electrostatic integrity, given the fact that they are controlled by a single-gate contact of length L_g=10.7 nm. Two findings should be highlighted: first, the 2-D materials with the highest mobility are not necessarily those with the largest ON-current because two terms contribute to their channel resistance $R_{ch} = R_{ball} + R_{diff}(L)$, a ballistic one, R_{ball}, that is length-independent and proportional to $\sqrt{m_{e/h}}$, and a diffusive one, $R_{diff}(L) = L/(q \cdot \mu_{ph}(\rho) \cdot \rho)$, that depends on the channel length L and on the inverse of the phonon-limited mobility μ_{ph} (q is the elementary charge and ρ the charge density). In ultra-short devices, the ballistic component dominates unless the mobility is very small, which explains the observed behavior in Fig. 3. Secondly, most ON-currents do not exceed 1 mA/μA, except in black phosphorus, the most promising 2-D crystal among the studied ones.

The simulations so far did not include the effect of contact resistances, which are known to be non-negligible (several k$\Omega \cdot \mu$m) in 2-D materials. While keeping the same *ab-initio* modeling approach as before a top-contact geometry with Titanium on MoS_2 has been assembled in Fig. 4 to address this critical issue. It is composed of three regions, which allows for an accurate extraction of the Schottky barrier (SB) height between the metal Fermi level and the pure MoS_2 only.

The SB alone does not explain the origin of the large contact resistances. To go one step further Fig. 5(a) illustrates the spectral current distribution through the Titanium-MoS_2 structure. It appears ordinary, as the electrostatic potential obtained from self-consistent Schrödinger-Poisson iterations. It shows an exponential decrease in the MoS_2 region, as in standard MOSFETs [20]. To get a deeper insight into the contact physics the spatial location of the current has also been examined in Fig. 5(b), where a transfer of about 20% of the total current from Titanium into MoS_2 occurs in the overlap region. A recent theoretical study using DFT suggested that 2-D semiconductors might get metalized when put in contact with certain metals such as Ti [21]. This could be the reason behind this current transfer.

However, our calculations do not support the metallization assumption. The latter would imply that the current magnitude at least slightly depends on the length of the metal-semiconductor overlap region, which is not the case here, as demonstrated in Fig. 5(c). Furthermore, although MoS_2 below the Titanium contact has a metal-like density-of-states (DOS), see Fig. 6(a), no metallization occurs since the band gap DOS simply results from the penetration of the metal wave function into the semiconductor. This is confirmed by directly injecting electrons into the MoS_2 layer in Fig. 4: the band gap DOS disappears, thus indicating that it is not the product of a MoS_2 metallization, but of evanescent states originating from the metal layer. These states are the reason for ∼20% of the total current flowing through MoS_2 instead of Ti in the overlap region. Still, the majority of the current is transferred from the metal into the semiconductor at the edge of the contact, contradicting a recent experiment where a transfer length of 630 nm was reported for MoS_2 with Ti/Au contacts [22].

Finally, Scandium and Gold contacts have also been simulated in Fig. 6, their Schottky barrier height extracted, and their contact resistance roughly estimated and compared to that of Titanium. As already predicted experimentally for multi-layer structures [23] Scandium emerges as the potentially best solution to reduce the contact resistance of single-layer MoS_2 devices due to the absence of a Schottky barrier.

IV. Conclusion

A detailed study of eight relevant 2-D materials has been described in this paper. It encompasses their electron and hole mobility, *I-V* characteristics, and contact resistance. According to available crystal databases, there exist 6,400 layered materials from which thousands of stable single-layer structures might be exfoliated. The same simulation approach as used here could be applied to those, even before they are experimentally isolated, to identify components capable of challenging Si MOSFETS or showing interesting features.

Acknowledgment

This work was supported by Swiss National Science Foundation Grant No. PP00P2_159314, by ETH Research Grant ETH-32 15-1, by the EU FP7 DEEPEN Project, and by a grant from the Swiss National Supercomputing Centre (CSCS) under Project s662. This research also used resources of the Oak Ridge Leadership Computing Facility at ORNL.

References

[1] K. S. Novoselov et al., Science 306, 666 (2004).
[2] B. Radisavljevic et al., Nat. Nano. 6, 147 (2011).
[3] D. Ovchinnikov et al., ACS Nano 8, 8174-8181 (2014).
[4] Y. Huang et al., ACS Nano 8, 10743-10755 (2014).
[5] L. Li et al., Nat. Nano. 9, 372-377 (2014).
[6] A. Allain and A. Kis, ACS Nano 8, 7180-7185 (2014).
[7] Z.-Y. Ong et al., Phys. Rev. B 88, 165316 (2013).
[8] A. Allain et al. Nat. Mat. 14, 1195 (2015).
[9] M. Luisier and G. Klimeck, Phys. Rev. B 80, 155430 (2009).
[10] G. Kresse and J. Furthmüller, Phys. Rev. B 54, 11169 (1996).
[11] A. A. Mostofi et al., Comp. Phys. Comm. 178, 685-699 (2008).
[12] A. Szabó et al., Phys. Rev. B 92, 035435 (2015).
[13] J. P. Perdew et al., Phys. Rev. Lett. 77, 3865 (1997).
[14] J. Heyd et al., J. Chem. Phys. 124, 219906 (2006).
[15] A. Togo et al., Phys. Rev. B 78, 134106 (2008).
[16] A. Szabó et al., Proc. of IEDM 2014, 30.4.1-30.4.4 (2014).
[17] A. Szabó et al., Proc. of IEDM 2015, 12.1.1-12.1.4 (2015).
[18] K. Rim et al., Proc. of IEDM 2002, 43-46 (2002).
[19] K. Kaasbjerg et al., Phys. Rev. B 85, 115317 (2012).
[20] J. Appenzeller et al., IEEE Trans. Elec. Dev. 55, 2827 (2008).
[21] J. Kang et al., Phys. Rev. X 4, 031005 (2014).
[22] H. Liu et al., ACS Nano 8, 1031 (2014).
[23] S. Das et al., Nano Lett. 13, 100 (2013).

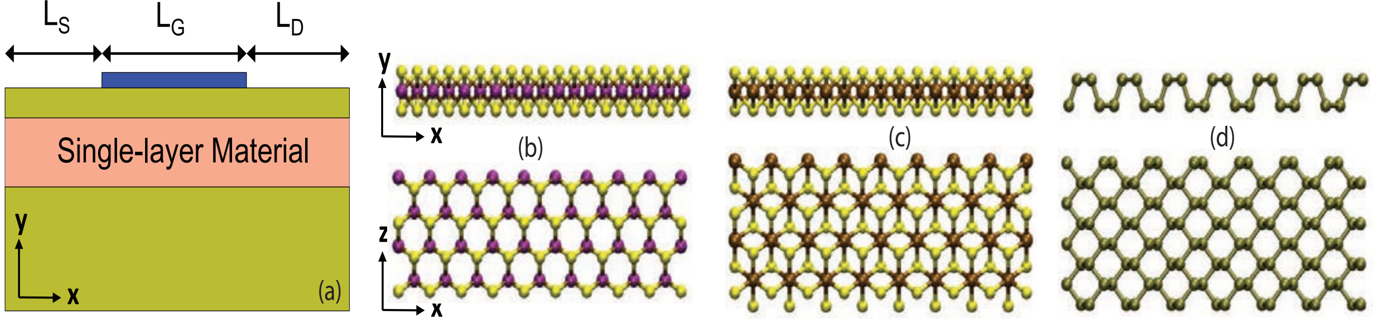

Fig. 1. (a) Schematic view of the investigated single-gate transistor with a 2-D monolayer semiconductor as channel. The source and drain extensions measure L_s=L_d=15 nm, whereas the gate length is set to 10.7 nm. High donor/acceptor concentrations ($N_{D/A}$ >1e13 cm^{-2}) are assumed in the source and drain regions to maintain excellent electrostatic properties. A t_{ox}=3 nm oxide layer separates the channel from the gate contact with a relative dielectric constant ϵ_R=20 and an equivalent oxide thickness of 0.58 nm. Transport occurs along the x-axis, y is the direction of confinement, and the third dimension, z, is modeled as periodic with 21 momentum points. (b-d) Side and top views of the 2-D crystal structures used in this work as transistor channels. (b) TMDs in the 2H phase (MoS_2, $MoSe_2$, $MoTe_2$, WS_2, and WSe_2). (c) Group IV dichalcogenide in the 1T phase (SnS_2). (d) Black phosphorus.

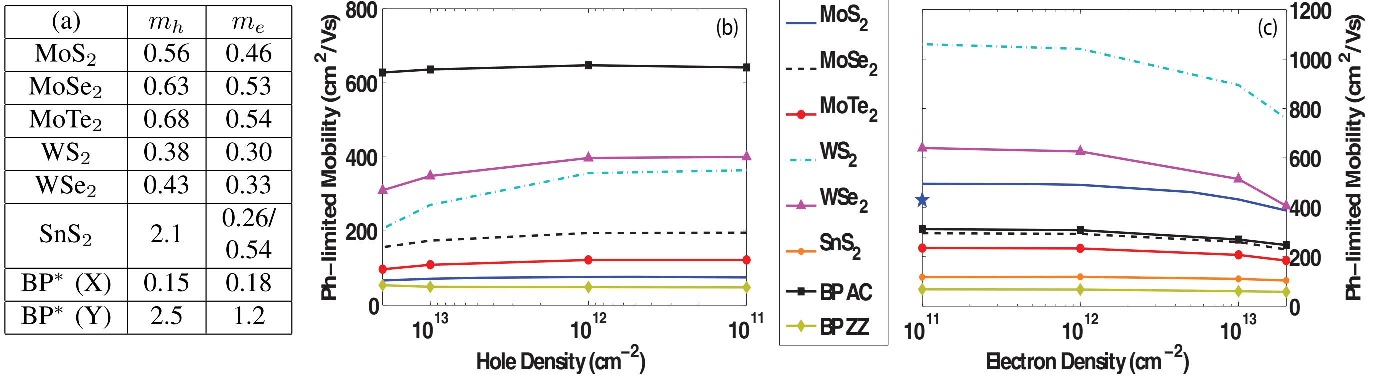

(a)	m_h	m_e
MoS_2	0.56	0.46
$MoSe_2$	0.63	0.53
$MoTe_2$	0.68	0.54
WS_2	0.38	0.30
WSe_2	0.43	0.33
SnS_2	2.1	0.26/ 0.54
BP* (X)	0.15	0.18
BP* (Y)	2.5	1.2

Fig. 2. (a) Table summarizing the electron (m_e) and hole (m_h) transport effective masses of the monolayer crystals considered in this paper. All data have been calculated with DFT using GGA as exchange-correlation functional [13], except black phosphorus, for which HSE06 hybrid functionals have been used [14]. Due to the anisotropy of the conduction band minimum of SnS_2 at the M point valleys with different effective masses contribute to transport. BP (X) indicates transport parallel to the armchair (AC) configuration, BP (Y) parallel to the zigzag (ZZ) one. (b) Low-field phonon-limited hole mobility vs. carrier concentration of the selected 2-D materials. All values were computed with the "dR/dL" method [18] and the *ab-initio* quantum transport approach based on MLWFs and briefly described in Section II. (c) Same as (b), but for the low-field phonon-limited electron mobility. The blue star refers to the phonon-limited mobility of electrons in single-layer MoS_2 as calculated with the linearized Boltzmann Transport Equation and DFT inputs (410 cm^2/Vs) [19].

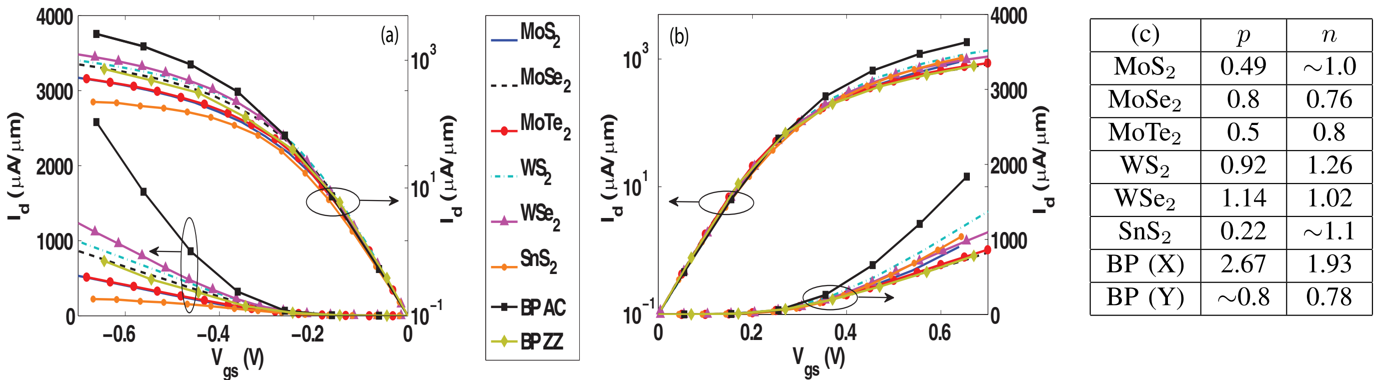

(c)	p	n
MoS_2	0.49	∼1.0
$MoSe_2$	0.8	0.76
$MoTe_2$	0.5	0.8
WS_2	0.92	1.26
WSe_2	1.14	1.02
SnS_2	0.22	∼1.1
BP (X)	2.67	1.93
BP (Y)	∼0.8	0.78

Fig. 3. (a) Intrinsic transfer characteristics I_d-V_{gs} (no source and drain contact resistances) at V_{ds}=-0.67 V of the single-gate transistor in Fig. 1 with a p-type configuration and with the 8 selected 2-D crystals as channel materials. Both a linear and a logarithmic scales are provided. The same color scheme as for the mobility in Fig. 2 has been applied. (b) Same as in (a), but for the n-type configuration at V_{ds}=0.67 V. (c) Table reporting the ON-current values (I_d at $|V_{gs}|$=$|V_{ds}|$=0.67 V) in mA/μm, as extracted from sub-plots (a) and (b). The entries preceded by a ∼ have been extrapolated from the available current data that do not go up to $|V_{gs}|$=0.67 V. The resulting inaccuracy in I_{ON} does not exceed 5%.

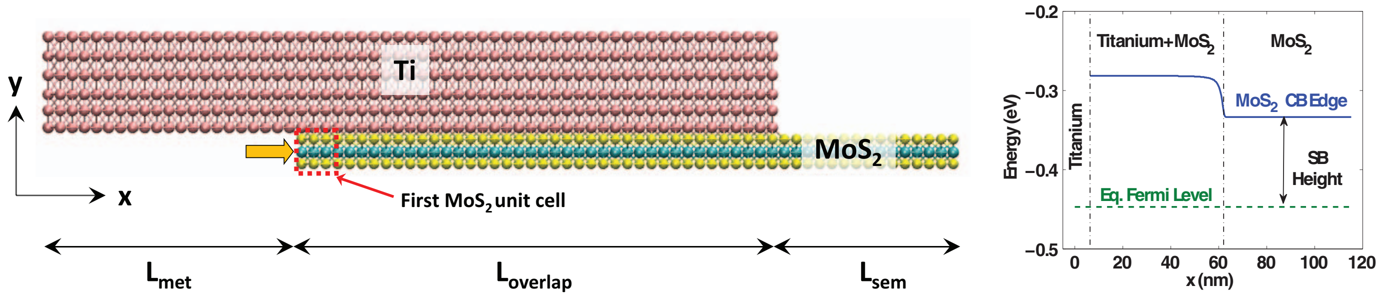

Fig. 4. (left) Schematic view of the metal-TMD geometry used to simulate the contact properties of single-layer MoS_2. Here, a Titanium layer is depicted. The constructed structures include three distinct regions, one with pure metal of length L_{met}, one where the metal and the TMD overlap of length $L_{overlap}$, and one with TMD only of length L_{sem}. Transport occurs along the x axis. In all calculations, L_{met}=6.5 nm and L_{sem}=55 nm, only $L_{overlap}$ varies. A back gate not shown here controls the electron flow through the metal-MoS_2 structure. It covers the entire device length. (right) Equilibrium band diagram of the atomic system illustrated on the left with $L_{overlap}$=55.7 nm. The Fermi level, the conduction band edge of MoS_2, and the Schottky barrier (SB) height are shown. The latter is extracted between the Fermi level of the metal and the region with pure MoS_2.

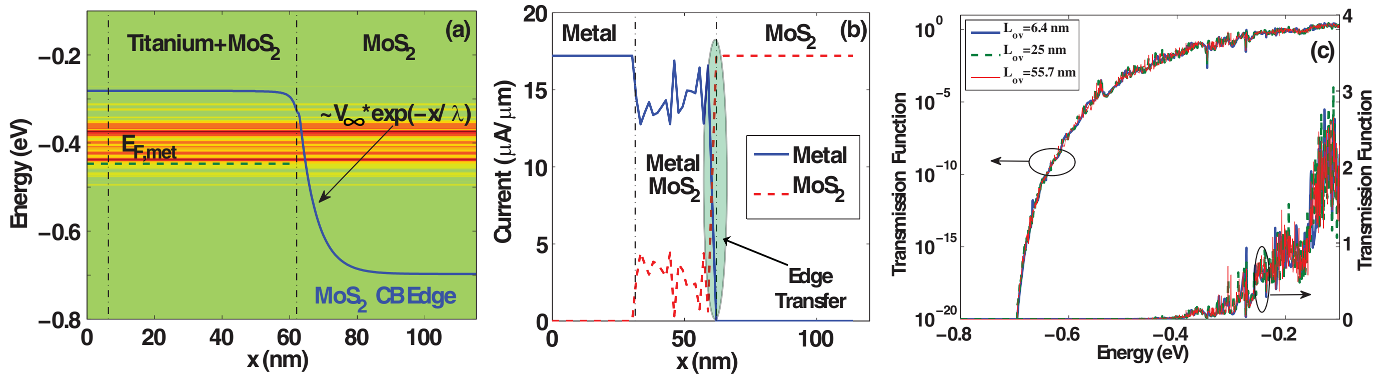

Fig. 5. (a) Spectral current flowing through the Titanium-MoS_2 structure in Fig. 4 with $L_{overlap}$=55.7 nm. Red indicates high current concentrations, green no current. The blue line refers to the conduction band of MoS_2, which has been pushed down by 0.35 eV in the pure MoS_2 region as compared to the equilibrium case in Fig. 4. A V_{ds}=0.5 V is assumed for the current calculations. The electrostatic potential profile in the MoS_2 part can be well approximated by an expression proportional to $V_{\infty}(1 + exp(-x/\lambda))$, where V_{∞} is the potential at large x and λ the screening length of the contact [20] that depends on the MoS_2 doping and electrostatics. (b) Current magnitude in the Titanium, Titanium-MoS_2, and MoS_2 regions in sub-plot (a). (c) Transmission function through the Titanium-MoS_2 structure as a function of the overlap length L_{ov}=6.4 (blue lines), 25 (dashed green lines), and 55.7 nm (thin red lines).

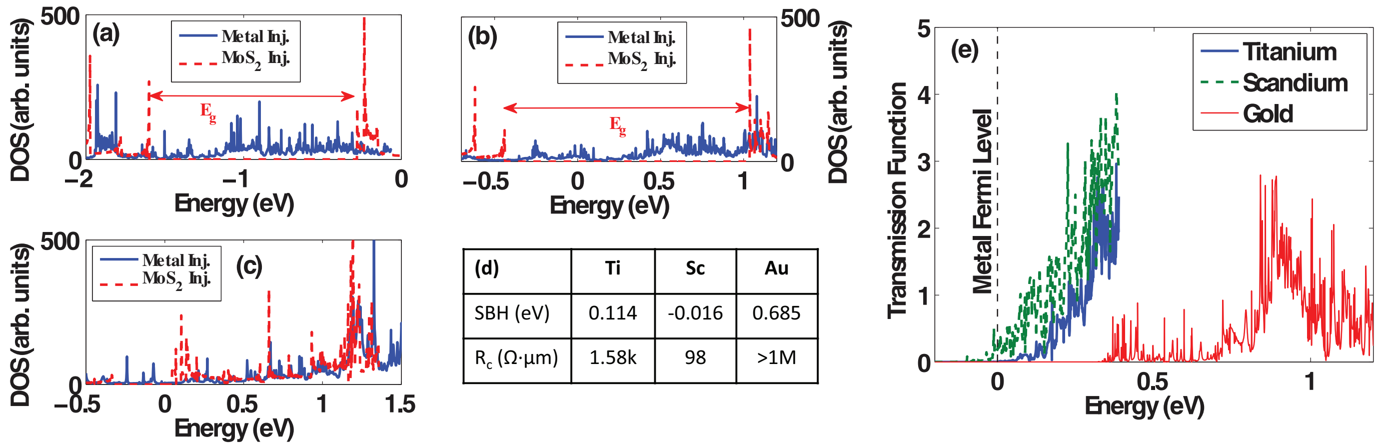

(d)	Ti	Sc	Au
SBH (eV)	0.114	-0.016	0.685
R_c (Ω·μm)	1.58k	98	>1M

Fig. 6. (a) Density-of-states in the first MoS_2 unit cell situated below the Titanium contact in Fig. 4 when the electrons are first injected into the top metal layer and then transmitted to MoS_2 (solid blue line) and when they are directly injected into MoS_2 along the orange arrow in Fig. 4 (dashed red line). (b) Same as (a), but with Scandium instead of Titanium. (c) Same as (a) and (b), but with Gold. A metallization of the MoS_2 monolayer takes place in this case, but with limited influence on the current. (d) Table summarizing the Schottky barrier height and the contact resistance R_c of Titanium, Scandium, and Gold for the top contact geometry of Fig. 4, λ=5 nm, and $E_{F,met}$-CB_{min,MoS_2}=0.25 eV, where CB_{min,MoS_2} is the minimum of the conduction band edge of the pure MoS_2 region. The R_c values are not quantitative. They only give a lower boundary for the contact resistance due to the approximations that have been made: ballistic transport, one single momentum point to model the periodic direction z, GGA exchange-correlation functional, ideal metal-semiconductor interface$\cdots$ (e) Transmission function through Titanium- (blue line), Scandium- (dashed green line), and Gold-MoS_2 (thin red line) contact geometries similar to the one plotted in Fig. 4 with $L_{overlap}$=6.4 nm. In all cases the characteristic screening length λ has been set to 5 nm, the metal Fermi level $E_{F,met}$ has been shifted to 0 eV and CB_{min,MoS_2} to -0.25 eV to allow for direct comparisons.